A LETTERS JOURNAL EXPLORING THE FRONTIERS OF PHYSICS

OFFPRINT

Shrinkage star-shaped cracks: Explaining the transition from 90 degrees to 120 degrees

G. GAUTHIER, V. LAZARUS and L. PAUCHARD

EPL, **89** (2010) 26002

A Letters Journal Exploring the Frontiers of Physics

January 2010

EPL, **89** (2010) 26002
doi: 10.1209/0295-5075/89/26002

www.epljournal.org

Shrinkage star-shaped cracks: Explaining the transition from 90 degrees to 120 degrees

G. Gauthier[1], V. Lazarus[2(a)] and L. Pauchard[3]

[1] *Univ Paris-Sud, UMR 7608, Lab FAST, Bat 502, Campus Univ - F-91405, Orsay, France, EU*
[2] *UPMC Univ Paris 6, UMR 7608, Lab FAST, Bat 502, Campus Univ - F-91405, Orsay, France, EU*
[3] *CNRS, UMR 7608, Lab FAST, Bat 502, Campus Univ - F-91405, Orsay, France, EU*

received 29 September 2009; accepted in final form 21 December 2009
published online 29 January 2010

PACS 62.20.M- – Structural failure of materials
PACS 91.60.Ba – Elasticity, fracture, and flow
PACS 83.80.Hj – Suspensions, dispersions, pastes, slurries, colloids

Abstract – Contraction due to drying or cooling of materials yields various self-organized crack patterns. The junctions between the cracks are complex and form in some conditions, star-shaped cracks with mostly 90 degrees or 120 degrees intersection angles. Any physical explanation of the selection of the angle is lacking. Here, we report directional drying of colloids experiments in capillary tubes allowing to obtain a reversible transition between 90 degrees and 120 degrees. We show that the transition is governed by a linear elastic fracture mechanics energy minimization principle hence by only one dimensionless parameter: the ratio between the Griffith length (balance between the energy needed to create cracks and to deform the material elastically) and the cell size. We give a straightforward characterization technique to estimate Griffith's length by changing the cell geometry. As a bonus, we deduce from it the toughness of drying colloidal suspensions. We underline that the method may be applied to a broad area of materials, from suspensions (colloids, paints or mud) to engineering (ceramics, coatings) and geological materials (basalt, sediments).

Introduction. – Giant's Causeway [1,2], Port Arthur tessellated pavement [3], Bimini Road [4], Mars polygons [5,6], septarias [7,8], fracture networks in muds, permafrost [9], paintings [10], gels [11], concrete [12], coatings are some more or less known examples of self-organized crack patterns that have intrigued people throughout history. These patterns are formed by constrained shrinking of the medium due, for instance, to cooling or drying leading to fracture. The crack networks form mostly 90° or 120° angles. Intersections at 90° angles form ⊤ or + shaped connections. ⊤ intersections are present in fracture networks formed in thin films due to sequential formation of the cracks [13]. The horizontal bar of the ⊤ is formed first and the vertical one later. On the other hand, + shaped connections are necessarily mostly formed simultaneously, since a crack cannot cross the free surface formed by another. They can be observed on Bimini Road formed by contraction of sedimentary rocks [4] or Port Arthur tessellated pavement (Eaglehawk Neck, Tasmania) (fig. 1(a)) whose formation is poorly understood but may be due to evaporation or cooling shrinkage of sedimentary rocks [3]. Intersections at 120° can be observed during the cooling of basalt [2]. They are formed simultaneously and appear as Y star-shaped connections. The Giant's Causeway, forming at some places a regular hexagonal tessellation (fig. 1(b)), is an example of such connections.

Intersections formed simultaneously, that is Y or + intersections, can be reproduced experimentally in different kinds of experiments. In experiments on drying of corn starch [14–16] or on cooling of ice [17], the fracture network is complex and forms a polygonal pattern with mainly Y intersections. + intersections have been observed in directional-drying experiments of colloidal suspensions in capillary tubes [18]. But to date, no experiments exist that allow to control the transition from Y to + intersections. In the lack of such experiments, previous theoretical predictions focused mainly on quasi-hexagonal crack patterns, in particular on their scaling [19–21] or the maturation of their shape [22–25]. In general, the hexagonal crack pattern is believed to be the solution of the energy minimization principle as in foams [22,26].

(a) E-mail: veronique.lazarus@upmc.fr

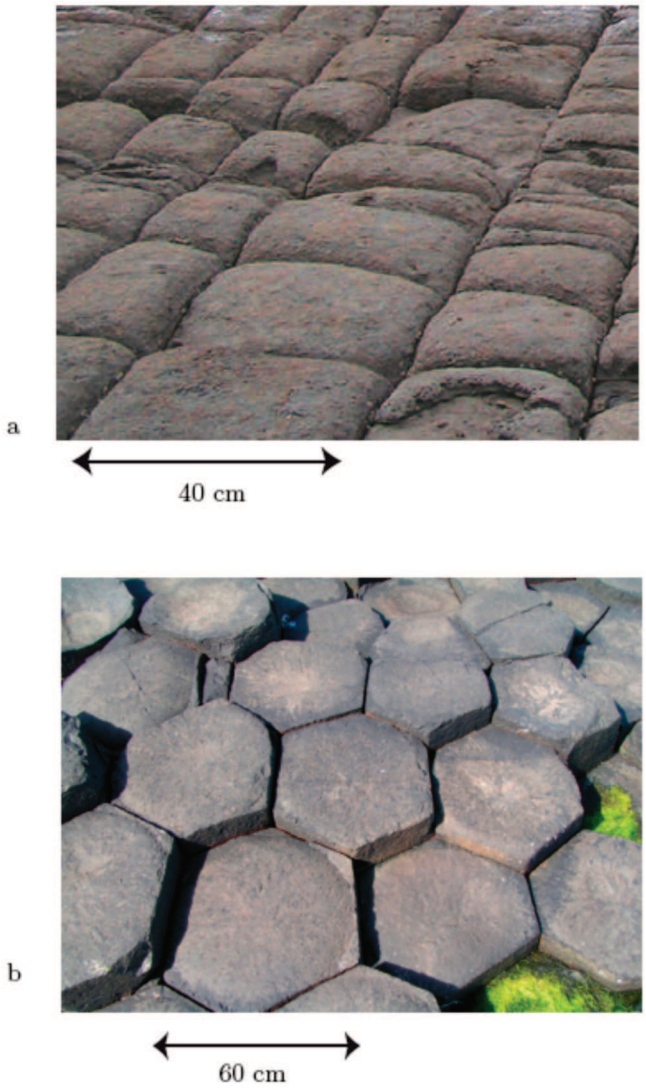

Fig. 1: (Colour on-line) Examples of polygonal patterns: (a) Port Arthur rectangular tessellated pavement, Tasmania (Courtesy of Wayne Bentley); (b) Giant's Causeway hexagonal tessellated pavement, Ireland (Courtesy of A. Davaille).

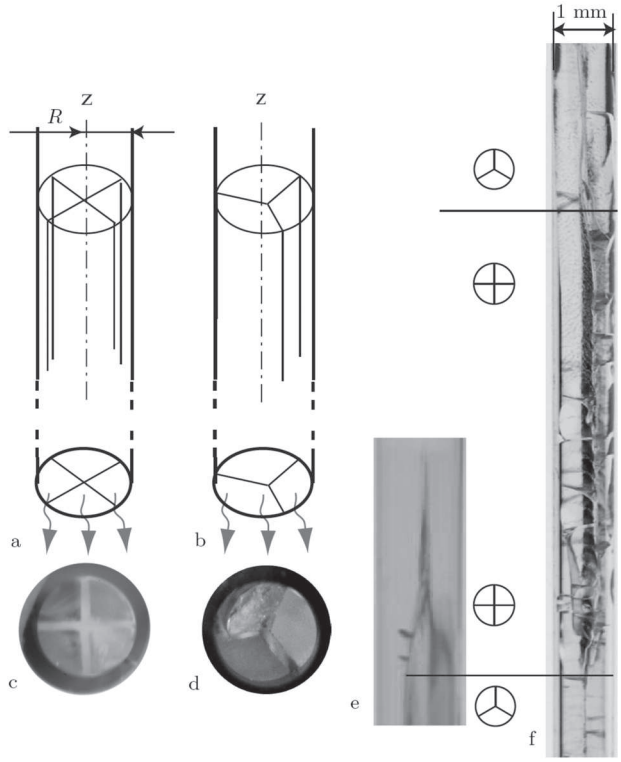

Fig. 2: The capillary tubes are filled with a colloidal suspension. The single bottom open edge allows for evaporation of the solvent. Cracks appear following the compaction front (front of the bottom-up growing gel). Their sectional shape depends on the controlled drying rate: (a,c) + intersection ($v \approx 64\,\mathrm{nm\,s^{-1}}$); (b,d) $\curlyvee$ intersection ($v \approx 31\,\mathrm{nm\,s^{-1}}$). (e,f) Pictures of the capillary tube at different times showing the reversible transition from $\curlyvee$ to + configuration: (e) the transition from $\curlyvee$ to + observed when the drying rate changes from $v \approx 31\,\mathrm{nm\,s^{-1}}$ to $v \approx 64\,\mathrm{nm\,s^{-1}}$; (f) followed by the transition + to $\curlyvee$ observed when the drying rate changes from $v \approx 64\,\mathrm{nm\,s^{-1}}$ to $v \approx 31\,\mathrm{nm\,s^{-1}}$ again (on this picture, the first secondary cracks have appeared explaining the finite observation scale).

In this letter, we report directional-drying experiments of colloidal suspensions in capillary tubes that allow to control the transition from $\curlyvee$ to + intersections. We show that the transition is governed by a Linear Elastic Fracture Mechanics (LEFM) energy minimization principle [27], hence by only one dimensionless parameter: the ratio between an internal length, the Griffith length, depending on the loading and the material, and an external length, the diameter of the tube. A straightforward method to estimate this parameter is given. This method is applied to the determination of the toughness of drying colloids (it seems that to date, only one such data exists [28]).

Experiments. – Directional-drying experiments are performed in circular capillary tubes [18], of length 12 cm and inner radius $R = 0.5\,\mathrm{mm}$, with an aqueous colloidal suspension (cf. fig. 2); namely Ludox® SM30 which is made of 30% in mass of silica spheroids particles of average diameter $2r = 7\,\mathrm{nm}$ (data given by the manufacturer Grace Davison). To ensure an unidirectional drying, the top extremity of each tube is closed. To balance the loss of water volume, tubes are only partially filled ($\approx 7\,\mathrm{cm}$ high) with suspension, so that the air trapped in the tube expands during the drying. After filling, the tubes dry in ambient condition for two hours, in order to form a 1 cm plug at the drying extremity, and then put in an airtight chamber. The drying rate is controlled either by the relative humidity RH or by the temperature T of the airtight chamber: changing T modifies the water viscosity and, according to Darcy's law, changes the water velocity through the porous medium formed by the gel. Experiments are performed at either 20 °C or 3 °C; the humidity rate is fixed either smaller than 10% using

desiccant or larger than 90% introducing water in the chamber.

Above the plug, vertical cracks appear that propagate following the compaction front (front of the bottom-up growing gel). These cracks are organized and clearly observable during a distance of propagation smaller than 3 cm. After this distance, the propagation becomes disordered and secondary cracks appear (fig. 2(f)). Experiments performed at $T = 20\,^{\circ}\mathrm{C}$ and $RH < 10\%$ give rise to 4 crack surfaces (fig. 2(a)), while drying at $T = 20\,^{\circ}\mathrm{C}$ and $RH > 90\%$ or at $T = 3\,^{\circ}\mathrm{C}$ and $RH < 10\%$ gives 3 crack surfaces. Changing the drying conditions changes the average velocity v of the crack tips. The velocities of the cracks tips are measured using a digital camera and are almost constant during the observation scale of the cracks (< 3 cm). Drying at $T = 20\,^{\circ}\mathrm{C}$ and $RH < 10\%$ corresponds to $v = 64 \pm 10\,\mathrm{nm\,s^{-1}}$, while drying at $T = 20\,^{\circ}\mathrm{C}$ and $RH > 90\%$ or at $T = 3\,^{\circ}\mathrm{C}$ and $RH < 10\%$ gives $v = 31 \pm 5\,\mathrm{nm\,s^{-1}}$. Errors on the velocity correspond to the scattering during one experiment and to the reproducibility on typically 10 experiments. Due to symmetry, the four cracks form a + connection. To check this point, the capillary tubes have been cut, at the crack tips, along a plane perpendicular to the tube axis (see fig. 2(c)). Similar cuts of tubes (fig. 2(d)) for slow-drying conditions ($v \approx 31\,\mathrm{nm\,s^{-1}}$) reveal a $\curlyvee$ shaped connection (fig. 2(b)). Changing the drying rate from $v \approx 31\,\mathrm{nm\,s^{-1}}$ to $v \approx 64\,\mathrm{nm\,s^{-1}}$ results in a reversible transition from + to $\curlyvee$ shape connections (fig. 2(e),(f)).

Fracture mechanics model. – From a mechanical point of view, the stationary behavior of the crack pattern in the crack tips reference frame allows to approximate the problem by using 2D plane strain linear elastic fracture mechanics. The medium is assumed to evolve quasistatically and to be subjected to a uniform isotropic tensile prestress σ_0 so that the Cauchy stress tensor $\boldsymbol{\sigma}$ is linked to the strain tensor $\boldsymbol{\varepsilon}$ by

$$\boldsymbol{\sigma} = \frac{E\nu}{(1+\nu)(1-2\nu)}\mathrm{tr}\boldsymbol{\varepsilon}\,\mathbf{1} + \frac{E}{(1+\nu)}\boldsymbol{\varepsilon} + \sigma_0\mathbf{1}, \qquad (1)$$

where E denotes the Young modulus and ν the Poisson ratio. The prestress σ_0 arises from the contraction of the medium due to capillary pore pressure in poro-elastic media during the drying process [29,30] and from thermal contraction during the cooling process [31]. Furthermore, our model assumes purely radial cracks, a perfect adhesion of the gel on the walls and traction-free boundary conditions on the cracks.

Then the local strain energy density $U(n)$ depends on the number n of radial cracks and is given as a function of the strain components ε_{ij} by (Einstein's implicit summation convention is employed for the indexes $i, j = 1, 2, 3$, see [31])

$$U(n) = \frac{E\nu}{2(1+\nu)(1-2\nu)}\varepsilon_{ii}^2 + \frac{E}{2(1+\nu)}\varepsilon_{ij}\varepsilon_{ij} + \sigma_0\varepsilon_{ii}. \qquad (2)$$

The total energy $\mathcal{E}(n)$, corresponding to the sum of the local strain energy and the crack energy, per unit height is

$$\mathcal{E}(n) = \int_S U(n)\,\mathrm{d}S + nG_cR\,. \qquad (3)$$

It depends on n, R, E, σ_0 and on G_c, which is the energy needed to create one unit area of crack [32]. Let us introduce the Griffith length L_c defined as

$$L_c = \frac{G_cE}{\sigma_0^2}. \qquad (4)$$

The dimensionless form [21] of $\mathcal{E}(n)$ reads

$$\frac{\mathcal{E}(n)E}{\sigma_0^2R^2} = \int_{\bar{S}} \bar{U}(n)\mathrm{d}\bar{S} + n\frac{L_c}{R}, \qquad (5)$$

where $\bar{S}$ is a the cross-sectional surface with $R = 1$ and $\bar{U}(n)$ is the local strain energy density in the presence of n radial cracks for a constraint elastic medium of unitary prestress $\sigma_0 = 1$, unitary Young's modulus $E = 1$ and radius $R = 1$.

Now we search among the radial crack configurations, the one that minimizes the total energy $\mathcal{E}(n)$ (some theoretical considerations about the principle can be found in [27,33]). Since the dimensionless form $\frac{\mathcal{E}(n)E}{\sigma_0^2R^2}$ of $\mathcal{E}(n)$ depends only on n and L_c/R (5), this minimization yields n_c as a function of a single dimensionless parameter L_c/R. L_c gives the ratio between the energy needed to create cracks ($\propto G_c$) and to deform the material elastically ($\propto \sigma_0^2/E$). The larger the critical energy release rate G_c (*i.e.* large value of L_c), the fewer the cracks. Hence the minimization of $\mathcal{E}$ in terms of n yields the critical number n_c as a decreasing function of L_c/R. This minimization is done numerically. For each given value of n, the mechanical stress and displacement fields, and then the strain energy density $\int_{\bar{S}} \bar{U}(n)\mathrm{d}\bar{S}$ corresponding to $E = 1$, $R = 1$ and $\sigma_0 = 1$ are calculated by finite elements using CAST3M. Minimization of (5) in terms of n yields n_c as a function of $\frac{L_c}{R}$. This function is plotted in fig. 3 for the typical value $\nu = 0.3$. It is a stairlike curve since the number of cracks can only be an integer.

Comparison with the experiments. – To compare numerical predictions with experiments, one needs to estimate Griffith's length L_c. For this, we use directional-drying experiments in flat (aspect ratio of $w/e = 20$, w being the width of the cell) Hele-Shaw cells [30,34], in the same drying conditions as above (cf. inset of fig. 4). The cells are 2 cm long for the 50, 100 and 200 μm thick, and 4 cm long for the ones of thickness 300 and 400 μm. The cells are half-filled with the suspension. During drying, a parallel array of cracks appears, with a crack spacing l which depends on the cell thickness e and the drying conditions. Applying again the minimization principle on these crack patterns, we obtain by 2D finite-elements computations, $l = a\sqrt{L_ce}$ with $a = 3.1$ for $\nu = 0.3$. The linear fit of l as a function of e gives the value of L_c

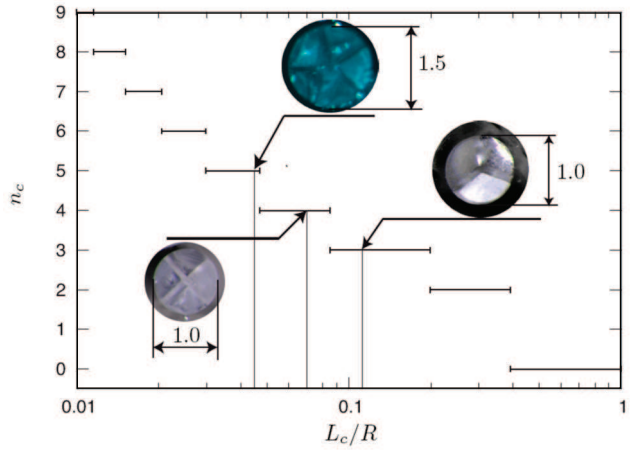

Fig. 3: (Colour on-line) Number of radial cracks in a capillary tube n_c as a function of Griffith's length L_c normalized with the radius of the capillary tube R ($n=1$ is not present for symmetry reasons) for $\nu=0.3$. The values are obtained by finite-element simulations: for each value L_c/R, the pattern with n_c radial cracks corresponds to the minimum of the total energy, which is the sum of the strain energy and the crack energy. Adhesion of the gel on the wall is supposed. The L_c/R and cross-section view of the experiments realized with Ludox® SM30 are shown.

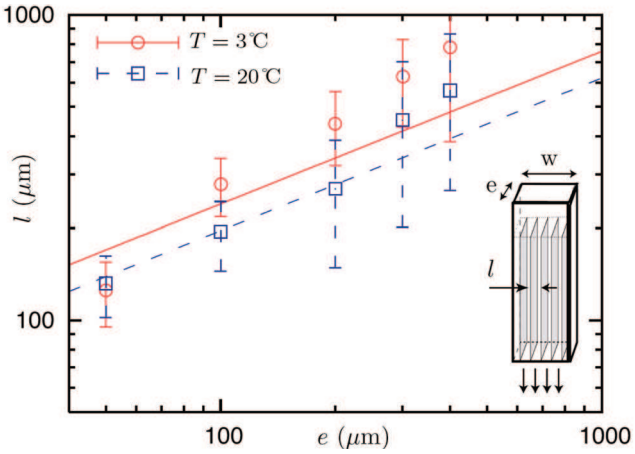

Fig. 4: (Colour on-line) Distance between cracks as a function of the thickness of the Hele-Shaw cell for drying of Ludox® SM30 at $T=3\,^\circ$C (○) and at $T=20\,^\circ$C (□). Griffith's length L_c is obtained by interpolation (lines) with the solution of the minimum-energy principle, that is $l=a\sqrt{L_c e}$, $a=3.1$ (obtained by FE for $\nu=0.3$). The linear fit is done systematically, in a least-square sense weighted by the error bars. The large scattering in the data points is due to the high variations in the crack spacing and the error bars correspond to the variability of l over more than 10 experiments.

for each suspension and drying condition: $L_c=60\pm18\,\mu$m for $v\approx31\,\mathrm{nm\,s^{-1}}$ and $L_c=34\pm10\,\mu$m for $v\approx64\,\mathrm{nm\,s^{-1}}$. Now reporting the corresponding values of L_c/R (0.12 and 0.068, respectively) on fig. 3 allows for the determination of n_c (3 and 4, respectively.) for the tube experiments. The predicted values are in good agreement with the experiments.

Moreover, the model predicts, for a fixed length L_c, that an increase of the radius R from 0.5 mm to 0.75 mm is expected to give rise to 5 radial cracks in the case $v\approx64\,\mathrm{nm\,s^{-1}}$: this transition is indeed observed ($L_c/R=0.045$ in fig. 3). The model also works for experiments on Ludox® HS 40 ($2r\approx12\,$nm). The values of L_c are then $L_c\simeq40\ \mu$m when drying rapidly and $L_c\simeq45\,\mu$m in cases of slow drying, and yield by minimization $n_c=4$ ($L_c/R=0.08$–0.09 in fig. 3) for both drying rates, that is a + shape intersection for $R\simeq0.5\,$mm, in agreement with the experiments. All these results allow to conclude that the transition between ϒ and + (and also 5 cracks) intersections is governed by energy minimization hence by the ratio of Griffith's length to the size of the cell.

Discussion. – Our study demonstrates that L_c depends on the drying rate. Several explanations can be proposed. The first explanation is that the stress σ_0 in the area of the crack tips is dependent on v because of diffusion effects [20]. The second explanation is that the porous medium formed by agglomeration of particles on the drying front has a different structure [35] as a function of v that induces a change of the values of E and G_c. The precise determination of the dependence of σ_0, E and G_c on the drying rate raises fundamental difficulties that are behind the scope of this article. We emphasize that by estimating directly L_c, we overcome these difficulties.

To simply derive L_c from Hele-Shaw experiments, the dependence of σ_0, that is L_c on the cell geometry, in particular on e, linked to 3D diffusion effects [25,36], has been neglected. The thicker the cells, the more important these effects are (fig. 4). Since [34], $l\propto e^{2/3}$, L_c varies as $e^{-1/3}$ which explains that the the slopes appear to be off in particular for larger values of e. But it can been disregarded here, e ranging from 50 μm to 400 μm, especially in the absence of more rigorous methods. For instance, the method consisting in translating measure of G_c and E from film measurements into directional drying is questionable, particularly since G_c and E are position and time dependent. Measuring L_c in the same kind of experiments overcomes these difficulties and allows to show that the transition between + and ϒ intersections is governed by the ratio of Griffith's length to the size of the cell.

The model can be used to estimate Griffith's length L_c. Since L_c depends on three parameters G_c, E and σ_0 (or two if one considers the mode I toughness defined by $K_{Ic}^2=\frac{E}{1-\nu^2}G_c$), this gives a method to obtain one parameter when the others are still known. For instance considering Ludox® SM30, assuming $\sigma_0=-2\gamma/r\simeq40\,$MPa, where $\gamma\simeq0.07\,$N/m is the air-water surface tension [30] and $2r=7\,$nm the particles diameter, the value of K_{Ic} can be derived from the measure of L_c: $K_{Ic}=\sigma_0\sqrt{L_c}\simeq0.2$–$0.3\,\mathrm{MPa\,m^{1/2}}$. This value seems reasonable compared to fused silica [37] for which $K_{Ic}\simeq1\,\mathrm{MPa\,m^{1/2}}$. It shall

however be noticed that it is significantly higher than the one often used in the literature for such material ($K_{Ic} \simeq 10^2\,\mathrm{Pa\,m^{1/2}}$ [28]). The discrepancy may be explained by the fact that the toughness seems to correspond to the fracture of solid/liquid interfaces in their experiments, and to the fracture of solid/solid ones in ours. Further discussion of this point is devoted to another article.

Conclusion. – We have observed a reversible transition $\curlyvee$ and + during directional-drying experiments in capillary tubes. We show that the selection between $\curlyvee$ and + intersections is controlled by the ratio of Griffith's length L_c to the diameter of the cell. It corresponds to a local minimum of the total energy, *i.e.* the sum of the elastic and crack energies. This is an experimental demonstration that the crack pattern satisfies the often used [21,22] principle of energy minimization. Directional-drying experiments in capillary tubes can be used to estimate Griffith's length L_c. Since L_c depends on three parameters G_c, E and σ_0 (or two if one considers the toughness defined by $K_{Ic}^2 = \frac{E}{1-\nu^2} G_c$), this gives a method to obtain one parameter when the others are still known. We applied it to estimate the toughness of consolidated Ludox®SM30. Extension from bounded to unbounded conditions is not straightforward and is the subject of further developments to infer new information on tessellated pavements formation on Earth or on other planets, as Mars where polygons are widely studied.

* * *

The authors thanks PPF *Processus physique en sciences de la terre* for funding, W. Bentley for the nice Port Arthur pictures, H. Auraldou, P. Gondret, N. Mangold, C. Maurini, E. Mittelstaedt, J. Levy and D. Salin for pertinent comments. The authors greatly appreciated A. Davaille comments and discussions on the geological patterns. The paper largely benefited from comments of referees.

REFERENCES

[1] O'Reilly J., *Trans. R. Ir. Acad.*, **26** (1878) 641.
[2] DeGraff J. M. and Aydin A., *Geol. Soc. Am.*, **99** (1987) 600.
[3] Branagan D. F. and Cairns H. C., *J. Proc. R. Soc. N. S. W.*, **126** (1993) 63.
[4] Shinn E. A., *Spec. Publ. Int. Assoc. Sedimentol.*, **41** (2009) 19.
[5] Mangold N., *Icarus*, **174** (2005) 336.
[6] Levy J., Head J. and Marchant D., *J. Geophys. Res.*, **114** (2009) E01007.
[7] Sellès-Martinez J., *Earth-Sci. Rev.*, **41** (1996) 177.
[8] Seilacher A., *Sediment. Geol.*, **143** (2001) 41.
[9] Plug L. J. and Werner B. T., *J. Geophys. Res.-Solid Earth*, **106** (2001) 8599.
[10] Pauchard L., Lazarus V., Abou B., Sekimoto K., Aitken G. and Lahanier C., *Reflets*, **3** (2007) 5.
[11] Atkinson A. and Guppy R. M., *J. Mater. Sci.*, **26** (1991) 3869.
[12] Colina H. and Roux S., *Eur. Phys. J. E*, **1** (2000) 189.
[13] Bohn S., Pauchard L. and Couder Y., *Phys. Rev. E*, **71** (2005) 046214.
[14] Muller G., *J. Geophys. Res.*, **103** (1998) 15239.
[15] Toramaru A. and Matsumoto T., *J. Geophys. Res.*, **109** (2004) B02205.
[16] Goehring L. and Morris S. W., *Europhys. Lett.*, **69** (2005) 739.
[17] Menger F. M., Zhang H., Caran K. L., Seredyuk V. A. and Apkarian R. P., *J. Am. Chem. Soc.*, **124** (2002) 1140.
[18] Gauthier G., Lazarus V. and Pauchard L., *Langmuir*, **23** (2007) 4715.
[19] Goehring L. and Morris S. W., *J. Geophys. Res.-Solid Earth*, **113** (2008) B10203.
[20] Goehring L., Mahadevan L. and Morris S. W., *Proc. Natl. Acad. Sci. U.S.A*, **106** (2009) 387.
[21] Jenkins D., *Int. J. Solids Struct.*, **46** (2009) 1078.
[22] Jagla E. A. and Rojo A. G., *Phys. Rev. E*, **65** (2002) 026203.
[23] Saliba R. and Jagla E. A., *J. Geophys. Res.-Solid Earth*, **108** (2003) 2476.
[24] Jagla E. A., *Phys. Rev. E*, **69** (2004) 056212.
[25] Bahr H.-A., Hofmann M., Weiss H.-J., Bahr U., Fischer G. and Balke H., *Phys. Rev. E*, **79** (2009) 056103.
[26] Weaire D. and Hutzler S., *The Physics of Foams* (Oxford University Press) 2000.
[27] Francfort G. A. and Marigo J. J., *J. Mech. Phys. Solids*, **46** (1998) 1319.
[28] Zarzycki J., *J. Non-Cryst. Solids*, **100** (1988) 359.
[29] Wang H. F., *Theory of Linear Poroelasticity with Applications to Geomechanics and Hydrogeology* (Princeton University Press, Princeton and Oxford) 2000.
[30] Dufresne E. R., Corwin E. I., Greenblatt N. A., Ashmore J., Wang D. Y., Dinsmore A. D., Cheng J. X., Xie X. S., Hutchinson J. W. and Weitz D. A., *Phys. Rev. Lett.*, **91** (2003) 224501.
[31] Timoshenko S. and Goodier J. N., *Theory of Elasticity* (McGraw-Hill, New-York) 1969.
[32] Griffith A. A., *Philos. Trans. R. Soc. London*, **221** (1920) 163.
[33] Bourdin B., Francfort G. and Marigo J.-J., *J. Elast.*, **91** (2008) 5.
[34] Allain C. and Limat L., *Phys. Rev. Lett.*, **74** (1995) 2981.
[35] Dong K., Yang R., Zou R. and Yu A., *Phys. Rev. Lett.*, **96** (2006) 145505.
[36] Hofmann M., Bahr H. A., Linse T., Bahr U., Balke H. and Weiss H. F., *Int. J. Fract.*, **141** (2006) 345.
[37] Michel M., Serbena F. and Lepienski C., *J. Non-Cryst. Solids*, **352** (2006) 3550.